EXPLORING URANUS THROUGH SCATTER

(SUSTAINED CUBESAT/CHIPSAT ACTIVITY THROUGH TRANSMITTED ELECTROMAGNETIC RADIATION)

NIAC Phase I Final Report

Grant number 80NSSC21K0691

Nicolas Lee, Sigrid Close (PI), Jared T. Blanchard, Kegan Kawamura, Benjamin Weldon, Michael Ying, and Sean A. Q. Young

Stanford University

2022 January 7

Abstract

We present a mission concept to study the capability for a parent spacecraft to transmit power and remotely manipulate a small probe spacecraft through a laser transmitter. This concept, entitled Sustained CubeSat Activity Through Transmitted Electromagnetic Radiation (SCATTER), enables the mothership to intermittently deploy probes to make distributed measurements where the use of only photovoltaic, battery, or radioisotope power sources would be infeasible. Using these probes during a long-duration deep space mission to Uranus would provide enhanced scientific measurements such as magnetic field gradients, leading to a better understanding of the ice giants, which are the least explored planets in our solar system.

In this report we assess the feasibility of using a mothership-based laser for wireless power transfer, translation and attitude control, and communication of probes ranging from a minimal-mass chipsat to a 3U CubeSat. We find that the best performance is achieved with an intermediate probe size, corresponding to a 0.5U CubeSat, which could capture over an order of magnitude more power than the chipsat, while being agile enough to maintain attitude control using laser photon pressure.

Table of contents

List of figures

Nomenclature

C_{L2}, C_{L3} = Jacobi constant at Lagrange points L2 and L3

F_{gBW} = gravity gradient force – beam width

F_{gZR} = gravity gradient force – z/R_{orb}

F_{gOOP} = out-of-plane gravitational force component

GM = gravitational parameter of Uranus (5,793,939 km^3/s^2)

I = irradiance

I_{amb} = ambient solar irradiance

P = captured power

P_{tot} = total output laser power

R = probe radius

R_{orb} = orbit radius around Uranus

R_U = Uranus planetary radius (25,362 km)

X = non-dimensional coordinate in 3-body system along the line between primary and secondary bodies

Y = non-dimensional coordinate in 3-body system in plane of primary and secondary bodies

a = semi-major axis of an orbit around Uranus

m = probe mass

r = transverse dimension to the laser beam (arbitrary direction in the plane)

w = beam radius

w_0 = beam waist radius

w_{max} = maximum laser beam width

x = transverse dimension to the laser beam (cartesian)

x_{COM} = probe center of mass position along the x dimension

z = dimension along the laser beam

z_R = Rayleigh length

z_{max} = maximum operating distance along the laser

λ = laser wavelength

θ = laser divergence angle

1 Introduction

We live in a time of unprecedented levels of exploration of our solar system. However, exploration of the outer planets remains infrequent and often is limited to flyby missions rather than orbiters. As a result, much remains unknown about the ice giants—Uranus and Neptune—and their interaction with the space environment. Uranus in particular is unique within our solar system because of its extreme axial tilt. As a result, direct measurements of its magnetosphere and plasma environment are of great interest to the planetary science community.

In this report, we present a concept to enable a conventional planetary orbiter to deploy and transmit power to companion probe spacecraft through an architecture entitled Sustained Chipsat/CubeSat Activity Through Transmitted Electromagnetic Radiation (SCATTER). This architecture, illustrated in Figure 1, enables small probes to be deployed intermittently through a long-duration deep space mission to make distributed measurements supporting the mothership spacecraft. Distributed small spacecraft deployed from a mothership can enhance a scientific mission by providing in situ measurements with greater geometric diversity. This architecture allows scientists to decouple temporal and spatial variations and address the myriad science questions pertaining to the ice giant magnetospheres and their evolution. Ideally, these probes would be capable of sustaining their own power generation by harvesting energy from the space environment. In some planetary environments, this could be achieved by harnessing natural phenomena such as the electromagnetic effects caused by plasma formed from hypervelocity impacts [1, 2], which would be frequent while operating in Saturn's rings [3], or the differential spacecraft charging resulting from immersion in a space plasma [4, 5] such as within the Io plasma torus.

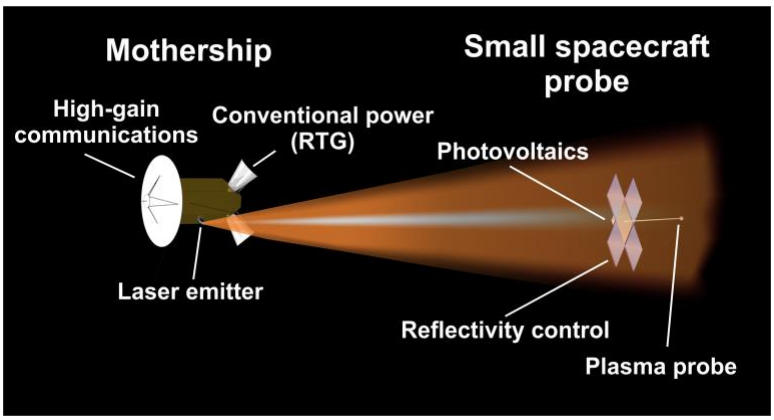

Figure 1: Illustration of mothership and probe subsystems in the SCATTER concept.

In the absence of sufficient energy provided by the space environment, laser power transmission from the mothership, derived from proposed wireless power transfer (WPT) technologies, allows probes to be deployed in locations where solar power is impractical and without the mass and cost of individual battery or nuclear power supplies for individual probe spacecraft. The power beam additionally provides an opportunity to further offload mass from the probe spacecraft by using reflectivity control devices to enable low-power and low-mass attitude control as well as data

transfer back to the mothership. Figure 2 shows a potential configuration with major subsystems of a chipsat-sized probe.

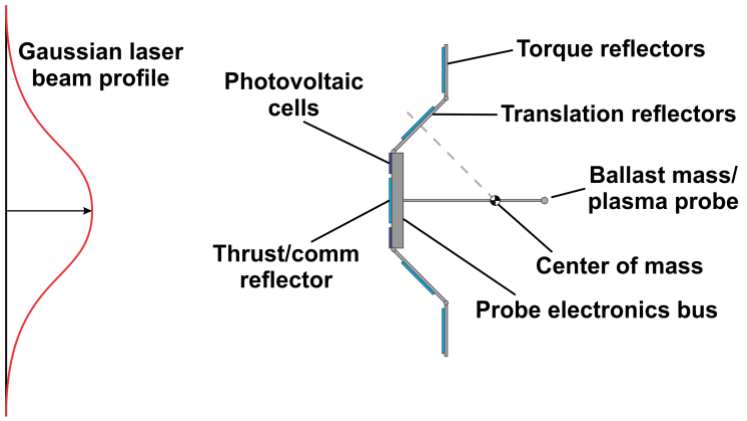

Figure 2: Potential configuration of chipsat-sized SCATTER probe.

1.1 Summary of NIAC Phase I results

The objective of the NIAC Phase I study was to demonstrate feasibility of the SCATTER architecture in the context of a magnetospheric study around Uranus, and to determine trends in SCATTER performance metrics as a function of probe size. Three specific probe sizes were analyzed: a 5 gram chipsat, 500 gram 0.5U CubeSat, and 5 kg 3U CubeSat.

The key findings from this NIAC study include the following:

- A laser emitter on the mothership with a 26 cm aperture and 25 W output power is sufficient to exceed solar irradiance to a distance of 1000 km.
- For probe sizes ranging from 5 grams to 5 kilograms, we find that an intermediate size corresponding to a 0.5U CubeSat achieves the best combination of performance metrics.
- With a 50 x 50 cm deployable membrane, the intermediate probe size is capable of maintaining laser-based attitude control within about 4 cm of the beam centerline.
- Assuming spring-driven deployment, probes will traverse the 1000 km distance in 1 to 6 days, with little effect on time-of-flight from radiation pressure.

1.2 Report outline

The remainder of this report is organized as follows. Section 2 will provide some background information on the Uranian system and prior spacecraft missions that are relevant to SCATTER. Section 3 will provide an overview of the mission concept to Uranus using a SCATTER payload. Section 4 and 5 will explore the design space available to the mothership subsystems and the deployed probes. Finally, Section 6 will summarize our major findings and provide a conclusion as well as directions for future study.

2 Background

2.1 Uranian planetary science

Among the scientific objectives laid out by the 2013–2022 Planetary Science Decadal Survey concerning the outer planets, the ice giants Uranus and Neptune are singled out [6]. While many planets in the solar system have been orbited by a scientific probe, the most distant planets have not. All extant data come from the brief flyby of Voyager 2 and telescopic measurements from Earth. Planetary scientists know very little about the evolution, energy balance, or detailed atmospheric and magnetospheric structure of these planets, which is expected to include rapid reconfigurations on a diurnal timescale [7]. In addition, the discovery of an abundance of exoplanets bearing similarities to the ice giants motivates a detailed understanding of analogues within our own solar system to draw meaningful conclusions about them [8].

Uranus orbits the Sun at a distance of 18.3 to 20.1 AU with an orbital period of 84 years. Its axial tilt of 97.9° and offset, tilted magnetic dipole (offset by 0.31 R_U and tilted 60° relative to the spin axis) result in a highly variable magnetosphere that follows the diurnal cycle with a period of 17.2 hours [9]. The Uranian bow shock and magnetopause occur with standoff distances of 23 and 18 R_U (583,326 km and 456,516 km), respectively [10]. These distances correspond closely to two of the five major Uranian moons: Oberon at 583,520 km and Titania at 435,910 km. The major moons orbit in the equatorial plane of Uranus, i.e. nearly perpendicular to the ecliptic.

During the flyby of Voyager 2 in 1986, the spacecraft collected magnetic field and plasma measurements using its suite of instruments, including low and high field magnetometers [11] and charged particle detectors [12, 13]. These measurements provide the basis of our understanding of the Uranian magnetosphere and its interaction with the impinging solar wind [14, 15], producing new findings even three decades later [16], but is limited by the trajectory of the spacecraft's single pass through the planetary system. Specifically, because of the previously unanticipated tilt of the magnetic dipole relative to the rotational axis of the planet, the solar wind did not impinge on the magnetosphere's cusp, even though Voyager 2's flyby coincided with a time when the rotational axis of Uranus was closely aligned with the sun direction.

Subsequent analysis of the data collected by Voyager 2 was used to build models of the magnetosphere and plasma environment around the Uranian system. These include the JPL Uranian Radiation Model [17] and the recent development of a multifluid magnetohydrodynamics model [18]. However, the dynamics predicted by these models can only hypothesize and predict the presence of specific phenomena, and a future mission would be required to provide confirmation through new measurements.

2.2 Distributed spacecraft measurements

Because of the highly dynamic nature of the Uranian magnetosphere, the measurements made by Voyager 2 have been difficult to interpret. In particular, temporal and spatial variations are challenging to decouple from measurements made using a single spacecraft platform. Distributed sensing using multiple spacecraft is one approach used in recent years to improve the science return

of a mission by decoupling spatial and temporal variations in measurements. The Cluster mission employed distributed sensing to explore the structure and dynamics of the Earth's bow shock and has since investigated other regions of the magnetosphere. The spacecraft are arranged in a tetrahedron, ranging from 40 km to 10,000 km. This large-scale separation has been used to probe phenomena that exist on those scales and to supplement models of the magnetosphere that sorely lack data for comparison [19]. THEMIS (Time History of Events and Macroscale Interactions During Substorms) operated on a similar principle, though with a different arrangement of spacecraft and different science objectives [20]. Both missions have demonstrated the value of this approach to space exploration in Earth's neighborhood, but the application to planetary exploration (and specifically using small spacecraft) has yet to be pioneered.

For planetary exploration, the cost of sending multiple conventional spacecraft to undertake a single mission can be prohibitive. The use of small spacecraft enables affordable deployment of constellations and swarms, which provide new capabilities for space exploration including distributed sensing to decouple spatial and temporal variations, enhanced robustness to individual failures, and increased geometric extent without the need for massive supporting structures. However, small spacecraft operate under severe constraints, including limited power and lifetime. An architecture that employs a single conventional spacecraft as mothership, supported by small spacecraft probes, takes advantage of the affordability of small spacecraft without sacrificing the capabilities associated with a conventional spacecraft.

2.3 Relevance to NASA, scientific community, and society

The SCATTER architecture supports NASA's 2018 Strategic Plan Objectives 1.1 and 3.1 by enabling exploration capabilities that will provide an improved understanding of the Uranian magnetosphere. It is also well aligned with the following areas of NASA's 2020 Technology Taxonomy:

- TX01.4.4: Propulsion systems – other advanced propulsion approaches;
- TX03.3.2: Aerospace power and energy storage – distribution and transmission;
- TX05.1.3: Optical communications – lasers;
- TX08.3.1: In-situ instruments and sensors – field and particle detectors; and
- TX17.3.4: Guidance, navigation, and control – control force/torque actuators.

Uranian magnetospheric measurements have a high priority in the exoplanet and outer planetary science communities and study of the icy giants was highlighted as a priority in the Planetary Science decadal survey [6]. The extreme tilt and offset of the Uranian magnetosphere results in a configuration with very different solar wind interactions from those at Jupiter and Saturn, which have been more extensively studied by Galileo and Cassini (and also through the New Horizons flyby of Jupiter). Exoplanets similar to Uranus and Neptune have been discovered, but our ability to understand the plasma environment around these highly tilted gas giants is limited by the scarcity of in situ measurements of the ice giants in our own solar system.

Planetary exploration has typically been associated with a high level of public interest and engagement, as demonstrated by the ever-increasing number of online viewers during landings on Mars, the popularity of the New Horizons image of Pluto on social media, and the Emmy Award presented to JPL for its coverage of Cassini's Grand Finale at Saturn. A proposed mission to Uranus involving new technologies would be expected to generate a similar level of interest from the general public.

If successful, SCATTER will prove beneficial to missions with the goal of making distributed measurements of the Uranian magnetosphere and other regions of the space environment even if the laser-driven aspect of SCATTER is not implemented. The experimental characterization of the probe payload subsystems will inform distributed spacecraft missions using independent power as well, since these requirements are independent of the power system implementation. SCATTER would enable exploration of the outer solar system, using small spacecraft to make distributed measurements, by providing a centralized power source and a communications relay for the probe spacecraft. The development of WPT technologies such as SCATTER will also be applicable to enhancing the robustness of fractionated spacecraft concepts for Earth-orbiting swarms and constellations. Spacecraft using SCATTER would have the potential to support each other in the event of power failures. Laser-based remote manipulation of objects in space can also have applications in space debris management in low Earth orbit. Development of WPT power collection and distribution systems and low-power scientific payloads would also be a first step toward enabling probes that are capable of sustaining their own power generation by harvesting energy from the space environment [3, 4, 5].

3 Mission concept

The many unanswered questions about the dynamics of the Uranian magnetosphere and its interaction with the solar wind provide motivation for prioritizing a future mission to study the system in greater detail. Compared to a single flyby, an orbiter can provide years of measurements and yield much greater insight into the diurnal and seasonal variations that are present. Several recent mission studies have been undertaken, including several New Frontiers class mission concepts [21, 22] as well as a menu of mission options ranging from New Frontiers to Flagship [23]. Each of these studies emphasized the need for instrumentation focused on magnetospheric studies, including magnetometers and energetic particle detectors.

The SCATTER architecture provides a method of powering CubeSat- or chipsat-class probes remotely using WPT from a mothership. With the capacity for a larger power source and larger antenna, this mothership can act as a relay for the measurements made by the smaller daughter spacecraft. The probes would be housed within the mothership during the cruise stage to Uranus. In orbit around Uranus, they would be dispensed sequentially from the mothership as required, targeting orbital regions such as the magnetospheric bow shock. The number of probes carried by the mothership is determined by the size and mass of each probe, which are constrained by performance requirements. Rather than generating power on board, the probes receive power from the mothership in the form of directed electromagnetic energy. The probes provide geometric

diversity in magnetospheric measurements until they reach a threshold separation distance where the beam power has significantly diverged. Voyager 2 showed plasma structure on the scale of ~1000 km that could be better resolved with distributed measurements [24]. The measurement period can last for several days, weeks, or months depending on the probe specifications.

The measurements themselves—magnetic field vectors, plasma density and temperature, and particle spectroscopy and composition—have a great deal of flight heritage. The Voyager 2 probe took measurements from four magnetometers, two boom-mounted and two on the spacecraft body. Extending the low field sensors several meters away from the spacecraft body allows for higher precision measurements of the planetary magnetic field since the sensors are further isolated from the fields generated by spacecraft electronics [11]. Many other exploratory spacecraft have employed this technique, including Cassini. Extending this to magnetometers onboard free-flying small spacecraft allows for complete separation from the parent spacecraft and more importantly, for simultaneous multipoint measurements. These probes, powered using SCATTER, can be magnetically clean, avoiding the disturbances inherent in measurements made by the parent spacecraft near its higher power subsystems. The power distribution network associated with the probe spacecraft can be operated at much lower currents and has a smaller geometry, resulting in less perturbation of the magnetic measurements.

For probes in the chipsat size range, in addition to providing power, the beam radiation pressure provides a mechanism for attitude control. Asymmetries in the surface reflectivity result in torques on the probe. Control of surface reflectivity, therefore, provides low-power attitude control for the probe, as well as translational control relative to the laser beam. If high frequency changes in surface reflectivity can be observed by optical instruments aboard the mothership, then the scattered laser light can be used to transmit data from the probe back to the mothership without an onboard radio and antenna. These additional innovations eliminate the need for a separate power source, propulsion system, attitude control system, and communications system for each probe, but require photovoltaics and reflectivity control devices. The effectiveness of these individual systems scale with different figures of merit associated with the probe geometry. A high-area design would provide visibility for communications to a greater distance, but greater mass and inertia would result in poor attitude control authority.

We expect that a nominal Uranus orbiter lifetime will be constrained primarily by the nominal design life of the RTG power source. The newest generation, known as the Multi-Mission Radioisotope Thermoelectric Generator (MMRTG) has a design life of 14 years [25]. JPL's Ice Giants mission study considered trajectories ranging from 8 to 12 years time of flight from launch to arrival at Uranus [23], which would allow for up to two to six years remaining on the RTG design life for a nominal primary mission. Based on the 59° tilt in the magnetic dipole of Uranus, the period of greatest interest from a magnetospheric perspective would be 1/6 of a Uranian year from its solstice (i.e in 2042 or 2056), when the magnetic dipole will rotate into and out of alignment with the sun direction on a diurnal cycle. Targeting a 2030–2033 launch could be challenging for a mission of this scale and with the SCATTER payload at a low level of

technological readiness; Cassini-Huygens, which launched in 1997, stemmed from plans for a Saturn orbiter that were initiated 15 years earlier in 1982 [26]. However, a 2043–2045 launch could be feasible to target a 2054 arrival, allowing for exploration of the magnetosphere over time as it progresses toward maximum alignment. During the primary mission, an initially circular orbit around Uranus at roughly 500,000 km radius would allow for multiple traversals of the magnetopause and solar wind bow shock. This orbital configuration would be agnostic to inclination, but would require the ascending or descending node to be aligned with the sun direction to explore the stagnation region of the bow shock. Such an orbit would have a period of approximately 9–14 days, and would be relatively slow in comparison to dynamics induced by the rotation of Uranus and its magnetic dipole, with a period of 17.23 hours. Subsequently, a highly elliptical orbit could be used to continue monitoring the magnetosphere and solar wind while exploring the inner regions of the Uranian system.

4 Mothership configuration

We assume that a Uranus orbiter will include a full suite of scientific instruments, and in this study, we focus on enabling distributed measurements specifically for studying the Uranian magnetosphere and its interaction with the solar wind. In particular, the SCATTER architecture requires the inclusion of a probe deployer and a laser emitter on the mothership. Here we present an initial outline of these subsystems in order to establish bounds on the performance of the deployed probes over a range of sizes, and we leave a detailed design of the mothership systems for future work.

4.1 Laser emitter

For our initial system design, we assume a Gaussian diffraction-limited laser beam emitted in a fixed direction from the mothership. The decision to use a laser-based WPT technology was primarily motivated by the comparatively low directivity of a microwave transmission system [27, 28]. Optical systems perform better over distances of up to 1000 km due to low beam divergence, despite the lower conversion efficiencies to and from electrical power. A wavelength of λ = 800 nm was chosen for demonstrated high efficiency power conversion, as described in more detail in Section 5.1.

Initial sizing of the laser emitter was selected to maintain an irradiance in the center of the beam greater than the ambient solar irradiance I_{amb} in Uranian orbit out to a separation of 1000 km. For a Gaussian beam intensity profile defined as

$$I(r) = \frac{2P}{\pi w(z)^2} \exp\left(\frac{-2r^2}{w(z)^2}\right) \tag{1}$$

with a laser power P and beam radius $w(z)$ at distance z along the beam and distance r transverse to the laser beamline, we can solve for the allowable beam width as a function of power:

$$w_{\max} = \sqrt{\frac{2P}{\pi I_{\text{amb}}}} \tag{2}$$

with I_{amb} = 3.69 W/m^2. Assuming a diffraction-limited divergence angle governed by

$$\theta = 1.22\frac{\lambda}{w_0} \tag{3}$$

for a beam waist radius w_0, we can solve for the beam waist required such that the beam profile at 1000 km distance has a peak intensity greater than ambient solar irradiance using the maximum beam width calculated in equation (2):

$$w_0 = 1.22\lambda\,\frac{1000\text{ km}}{w_{\max}}. \tag{4}$$

The maximum beamwidth $w_{\max}$ and required waist radius w_0 are plotted as a function of output laser power in Figure 3.

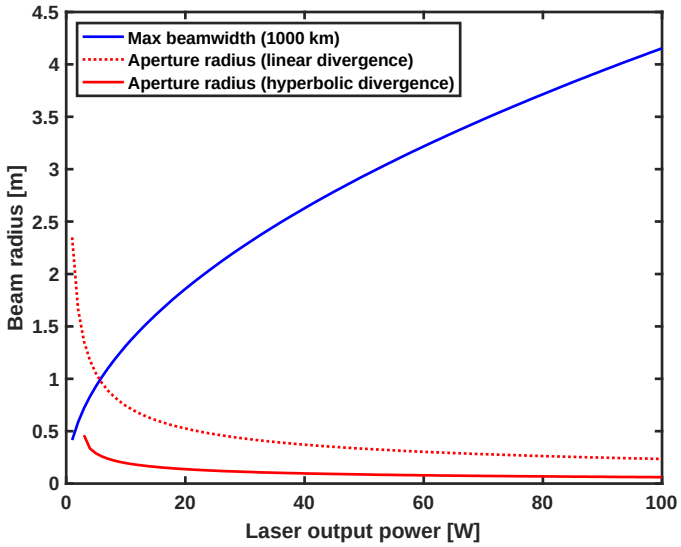

Figure 3: Maximum beamwidth at 1000 km in blue and aperture radius in red assuming linear divergence (dotted) and hyperbolic divergence (solid), corresponding to a diffraction-limited beam with peak irradiance at 1000 km exceeding ambient solar conditions.

As expected, as laser power increases, the allowable divergence angle also increases, and the required waist can be smaller. However, for a given wavelength and beam waist, the Rayleigh length (the distance along the beam from the waist to a doubling of the beam area) is governed by

$$z_{\text{R}} = \frac{\pi}{\lambda}w_0^2 \tag{5}$$

as plotted in Figure 4.

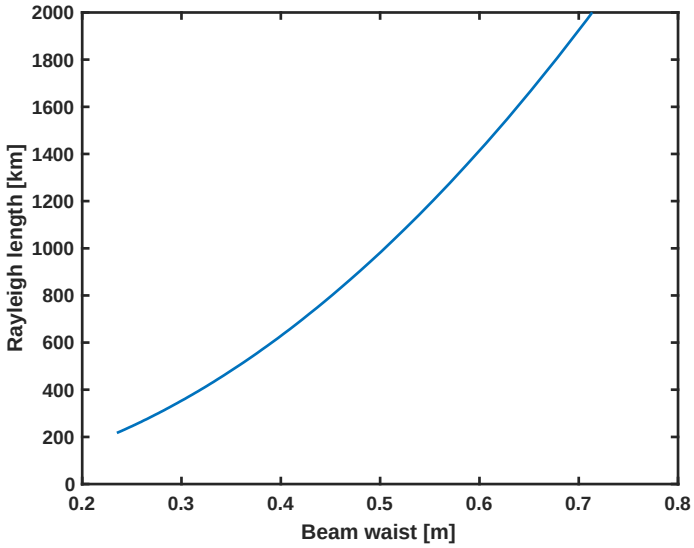

Figure 4: Rayleigh length corresponding to beam waist.

Here we can see that the Rayleigh length exceeds 1000 km for any beam waist exceeding 0.5 m radius. As a result, the evolution of beam width in the region of interest is better governed by the hyperbolic relation

$$w = w_0\sqrt{1+\left(\frac{z}{z_R}\right)^2} \tag{6}$$

rather than the asymptotic divergence angle [29]. For this case, if we set the beam width at z_{max} = 1000 km to w_{max}, we get a quadratic equation in w_0^2:

$$w_0^4 - w_{max}^2 w_0^2 + \frac{z_{max}^2\lambda^2}{\pi^2} = 0. \tag{7}$$

Now we can explicitly solve for

$$w_0 = \sqrt{\frac{1}{2}\left(w_{max}^2 - \sqrt{w_{max}^4 - \frac{4z_{max}^2\lambda^2}{\pi^2}}\right)}, \tag{8}$$

so long as

$$w_{max} > \sqrt{\frac{2z_{max}\lambda}{\pi}} \approx 0.714 \text{ m}. \tag{9}$$

Equation (8) is also plotted in Figure 3, showing a smaller required aperture based on the hyperbolic divergence geometry. This yields w_0 = 0.128 m as the minimum beam waist for a 25 W diffraction-limited laser.

Figure 5 shows the beam profile as a function of distance for three different beam waists. While the beam waist of 0.128 m provides the absolute minimum laser intensity at a distance of 1000 km to maintain irradiance greater than the ambient solar irradiance, we will assume a waist of 0.25 m radius for the remainder of this study to allow for some margin in the laser system.

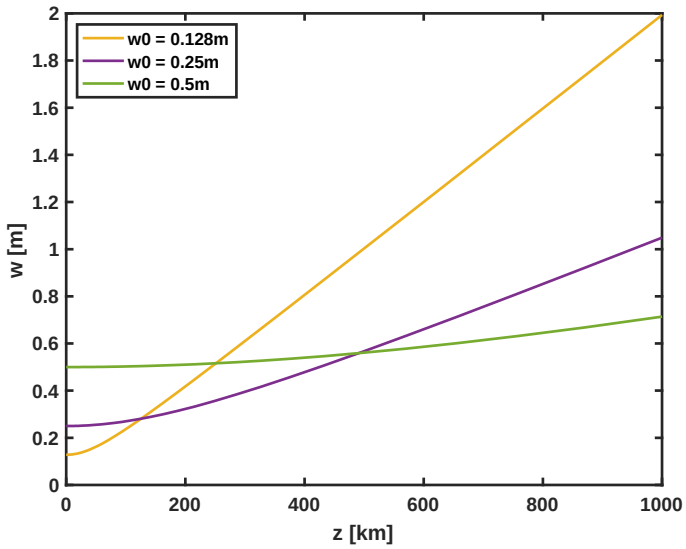

Figure 5: Beam width as a function of distance for three different beam waists, showing the difference in divergence angle.

The conversion efficiency of a laser system is typically assumed to be approximately 50% [30]. For a 25 W laser output power, we therefore require 50 W of electrical power from the mothership. In comparison, Cassini's three RTGs provided 887 W_e at the beginning of the mission, dropping to 640 W_e after 16 years [31]. If a Uranus orbiter were similarly powered, the laser emitter would consume no more than 10% of the available spacecraft power.

Assuming that the beam waist corresponds to the aperture size of the laser emitter, the minimum waist size of 0.128 m radius is similar to apertures used in laser communications payloads with flight heritage, including the 25 cm SILEX (Semiconductor-laser Intersatellite Link Experiment) payload launched on SPOT4 and Artemis in 2001 [32] and the 26 cm Laser-Utilizing Communications Equipment (LUCE) payload on the Optical Inter-orbit Communications Engineering Test Satellite (OICETS) launched in 2005 [33, 34]. Using a larger aperture laser would incur a mass and volume penalty, but advances in active control of lightweight deformable optics [35], as well as deployable optical elements [36] could potentially offset much of this penalty.

We expect that a coarse pan/tilt mechanism associated with the laser optics would still be required to set the laser orientation relative to the spacecraft prior to activating the laser and deploying a probe. Having this actuation authority would allow flexibility in maintaining the laser and probe orientation while satisfying other mission constraints, such as keeping the high gain antenna oriented toward Earth. However, because of the large size of the laser optics, we expect that the emitter will remain pointing in a fixed direction relative to the mothership chassis while in operation. This offloads the need for pointing control to the mothership attitude and determination system, and avoids the complexity of shifting the spacecraft mass properties while maintaining a precise orientation. With a fixed laser beam orientation, the requirement of keeping a probe centered in the beam falls on the probe itself, which must have sufficient translational authority to regulate its beam-relative position.

4.2 Probe storage and deployment

In addition to the laser emitter, the mothership is responsible for housing the probes in a deployer that can inject probes one by one into the activated laser beam. To maintain alignment with the laser, this deployer and likely the entire probe storage compartment would be mounted on the same pan/tilt mechanism as is used for laser orientation relative to the mothership. The mechanical design of a deployer mechanism would depend strongly on the size of the probe, over the range of sizes considered in the following section. In general, if the laser optics use a Cassegrain configuration similar to the LUCE optical antenna [34], the secondary mirror mount could also host the probe deployer in a coaxial configuration, such that probes are injected directly along the beam centerline. This would only be feasible for smaller probe designs where the size of the deployer does not exceed the size of the secondary mirror.

For probes that are larger in size, individual canistered housings with integrated deployers can be positioned adjacent to the laser emitter and inject the probes at a slight angle into the beam. This type of deployer would be similar to a conventional CubeSat deployer such as the Poly Picosatellite Orbital Deployer (P-POD) developed by CalPoly [37]. For a greater number of smaller probes, using individual deployers for each probe would scale poorly, and a single deployer that can load individual probes from a cartridge would be more efficient. In either case, deployment would be achieved by stored spring energy. Spring-loaded deployers for CubeSats impart typically about 1.5 m/s deployment speed [37], while a custom deployer for a smaller probe would potentially be able to achieve higher speeds.

4.3 Orbital configuration

The mothership's orbit will be dictated by overall mission and scientific drivers beyond the magnetospheric study that is addressed by the SCATTER probes. However, for the magnetosphere to be effectively characterized, at least part of the mission duration must include an orbit that traverses the bow shock and magnetopause, located at approximately 23 and 18 planetary radii (583,326 km and 456,516 km), respectively. Because of the proximity of two major moons orbiting at nearby distances, we consider the effect of three-body gravitational dynamics on the

mothership trajectory. For two circular reference orbits at a = 456,516 km and a = 583,326 km, corresponding to orbital periods of 9.3 and 13.5 days, Figure 6 shows the possible range of gravitational accelerations from Uranus and its five major moons. For the smaller orbit, Titania has the greatest secondary effect, which is still almost two order of magnitude less than the acceleration from Uranus. For the larger orbit, Oberon's gravitational pull can exceed that of Uranus if the probe lines up with Oberon.

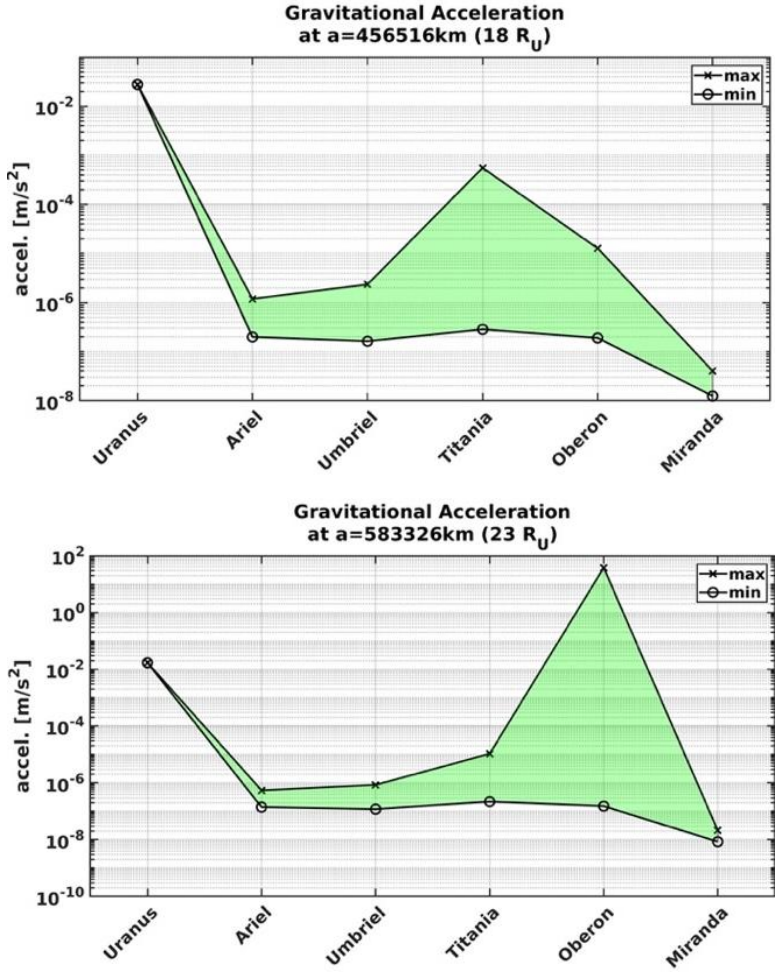

Figure 6: Maximum and minimum contributions to gravitational acceleration at 18 R_U (top) and 23 R_U (bottom) from Uranus and its five major moons.

To assess the potential influence of these major moons, we assume that the mothership operates in an orbit co-planar with the moons, where they would have the greatest gravitational influence over the trajectory. Three-body gravitational effects can impart drastic changes to a spacecraft's trajectory. In some cases, this can be desirable, for producing low-thrust trajectories that enable capture and landing on the secondary body [38, 39]. However, for the purpose of planetary protection, we desire trajectories where probes will not interact with the moons of Uranus and potentially land. Figure 7 shows a potential trajectory governed by the gravitational dynamics of a circular restricted three-body problem (CR3BP) relative to Uranus and Titania. The CR3BP

defines motion of a body of negligible mass (i.e., the spacecraft) in a rotating frame aligned with two large gravitational masses (in this case, Uranus and Titania). For the 18 R_U orbit that is near Titania's orbit, the Jacobi constant is 3.0016. This is between C_{L2} and C_{L3}, so the forbidden region, where the spacecraft cannot enter without a change in energy, will have a gap near Titania. Integrating a potential circular orbit in the CR3BP with Titania as the secondary body shows that the moon can produce a substantial disturbance to the mothership's trajectory in this orbit, even causing collision.

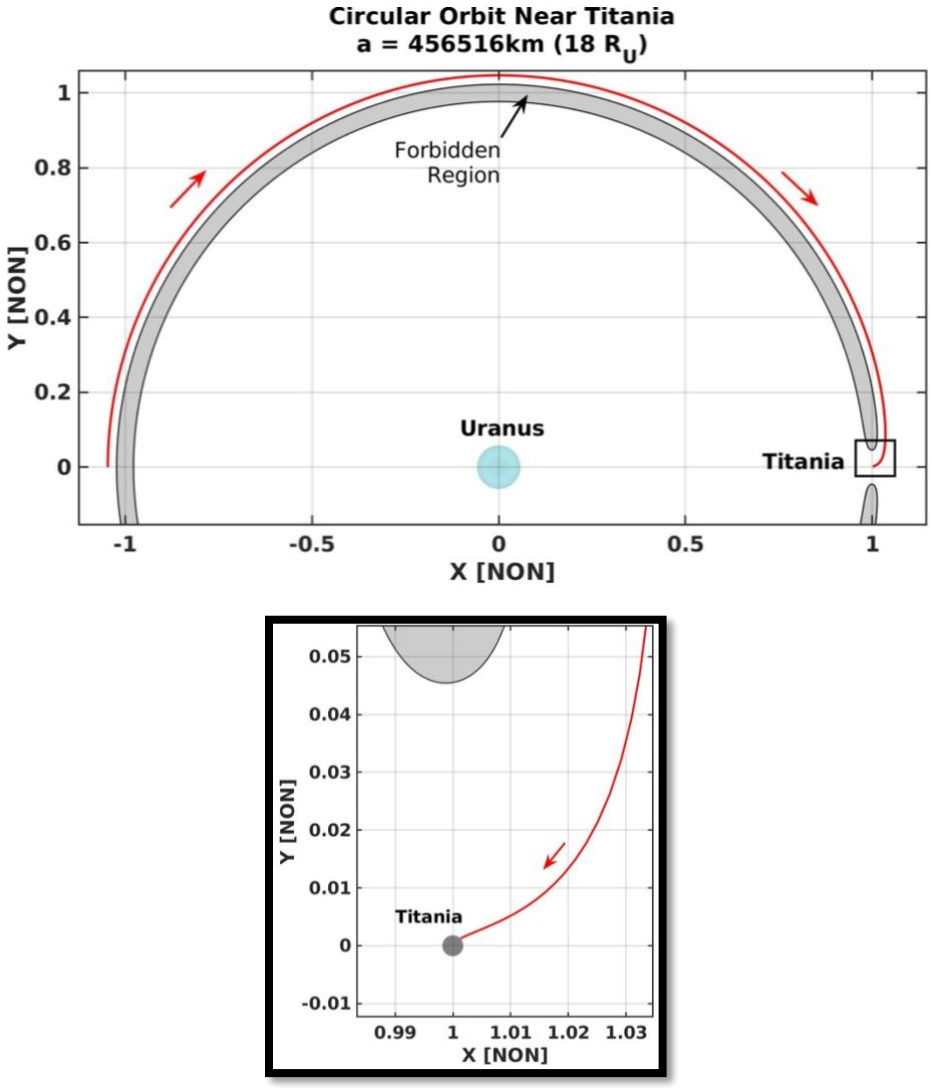

Figure 7: Three-body trajectory starting at a 456,516 km circular orbit and initially opposite Titania. Lengths are nondimensionalized by Titania's orbital radius. The inset (below) shows the final approach of this trajectory as it intersects with Titania.

For the Uranus–Oberon case, the trajectory at 23 R_U has a lower Jacobi constant (higher energy) but there is still a forbidden region, as shown in Figure 8 (inset). Using a semimajor axis of

583,326 km, the period is so close to that of Oberon's that the mothership can effectively stay on the opposite side of Uranus all the time and avoid the gravitational effect of Oberon. A similar selection of orbital period similar to Titania would provide the same solution for the 18 R_U case. Figure 8 (top) shows an orbit integrated for 214 days. The mothership remains near its initial location near X = -1 in the rotating system over this entire duration, slowly drifting away from the L3 Lagrange point. Obviously, the result would be very different if the trajectory began nearer to Oberon rather than on the opposite side of Uranus.

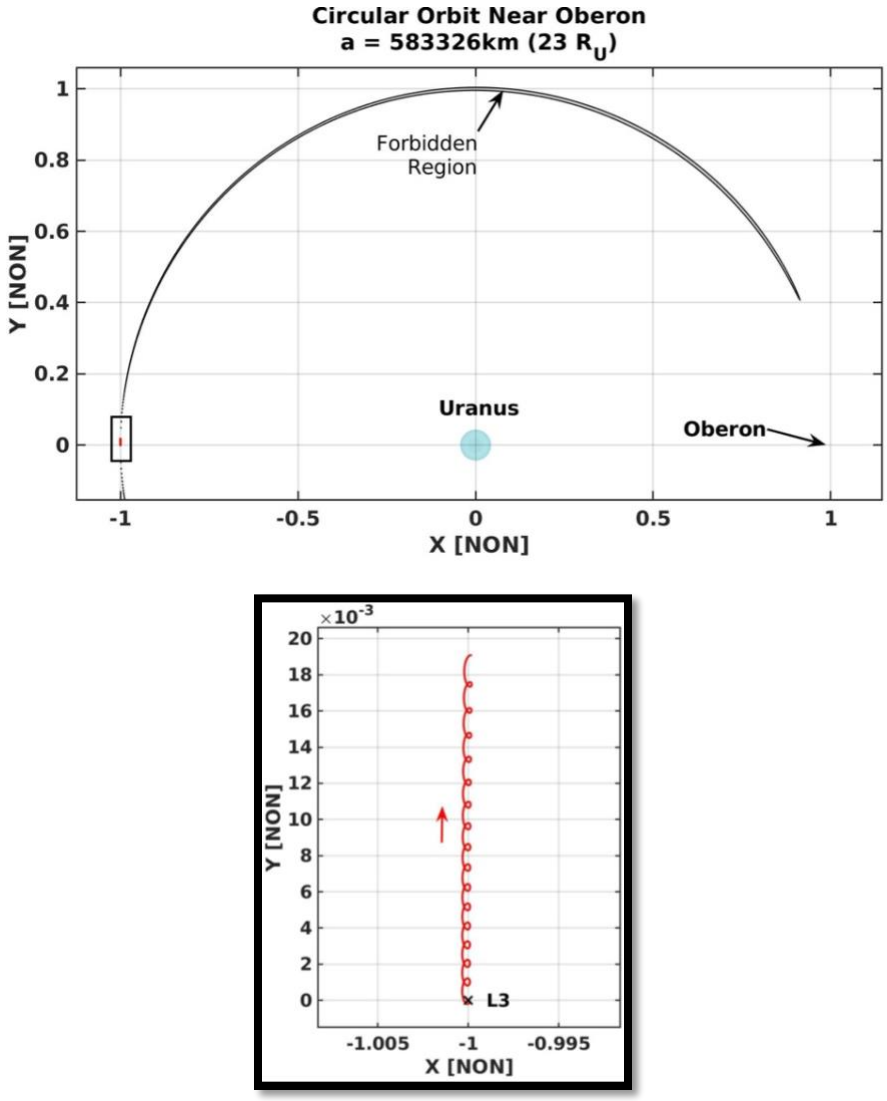

Figure 8: Three-body trajectory starting at a 583,326 km circular orbit and initially opposite Oberon. Lengths are nondimensionalized by Oberon's orbital radius. The inset shows the trajectory integrated over 214 days, remaining opposite to Oberon.

The two reference circular orbits considered in this section are only a preliminary analysis to gauge the potential influence of the moons nearest to the region of interest at the distance of the

bow shock and magnetopause. In general, a wide range of orbital options can be considered, including elliptical orbits and those that are not coplanar with the Uranian moons. A more detailed orbital design, which is beyond the scope of this study, would also need to account for the requirements of multiple scientific goals rather than just enabling distributed measurements of the Uranian magnetosphere.

5 Probe design

In this section, we assess the performance of the SCATTER architecture applied to a range of probe sizes and masses from a minimal chipsat design to a 3U CubeSat. In each case, we assume that the mass of the probe is concentrated in a small bus, with deployed membrane structures to increase the collecting area with minimal additional contribution to the probe's moment of inertia. This deployable collector may be packaged as discrete hinged panels, in the case of the smaller designs, or could use spiral wrapping techniques that accommodate multiple layers [40] and membrane thickness [41, 42] to efficiently package larger collectors. Three specific point designs will be used for the subsequent analysis: for the minimal chipsat, we consider a 4×4 cm planar bus with a 10 cm membrane collector and a total mass of 5 g; the largest CubeSat configuration we consider is a 5 kg 3U CubeSat bus (10×10×30 cm) that deploys a 2 m membrane collector; we also consider an intermediate design of a 50 cm collector on a 500 g 0.5U CubeSat bus (10×10×5 cm). However, to reduce the complexity of the analysis, we will make simplifying assumptions where appropriate about the geometry of the spacecraft to obtain trends in performance. For example, in Section 5.1 we use a circular probe geometry to simplify the integral while in Section 5.3 we assume a square geometry. The goal here is to obtain rough figures of merit and assess trends in performance, and not to specify a detailed design of the probe geometry.

5.1 Power transfer

There have been many prior studies of mission concepts involving laser power transfer. Many of these concepts apply higher power laser systems over shorter distances, such as a 250 W laser over 50 m for a rover to explore a darkened lunar crater [30], or 300 W transmitted over 1 km for a space elevator climber [43].

Given the 25 W laser with 0.5 m diameter waist as selected in Section 4.1, the total power from the laser beam impinging on the probe surface is estimated by integrating the power density over a circular disc centered on the beam axis. For the three point-design sizes of R = 1 m, R = 25 cm, and R = 5 cm, the power captured as a function of distance from the mothership is shown in Figure 9. The largest probe spans a capture area larger than the laser beam for much of this region, and therefore captures the full 25 W output of the laser, falling to 20 W at 1000 km. The smallest probe starts out already much smaller than the laser beam and therefore captures much less power, starting at 2 W on deployment and falling to just over 100 mW at 1000 km. The intermediate design ranges from about 21 W down to nearly 3 W at 1000 km.

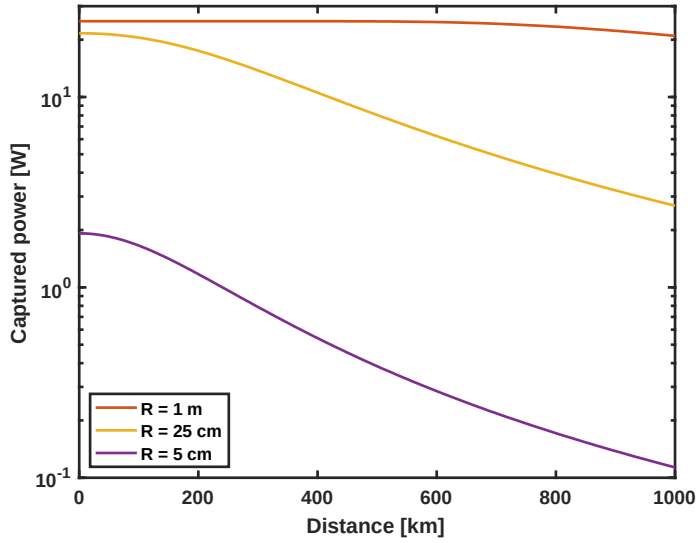

Figure 9: Integrated power from the laser beam impinging on a circular disc aligned with the beam center. Captured power as a function of distance for three specific probe sizes.

Figure 10 shows the captured power over a range of probe sizes at 1000 km from the mothership, providing greater resolution of the minimum power configuration as a function of probe size than the three design points considered in Figure 9.

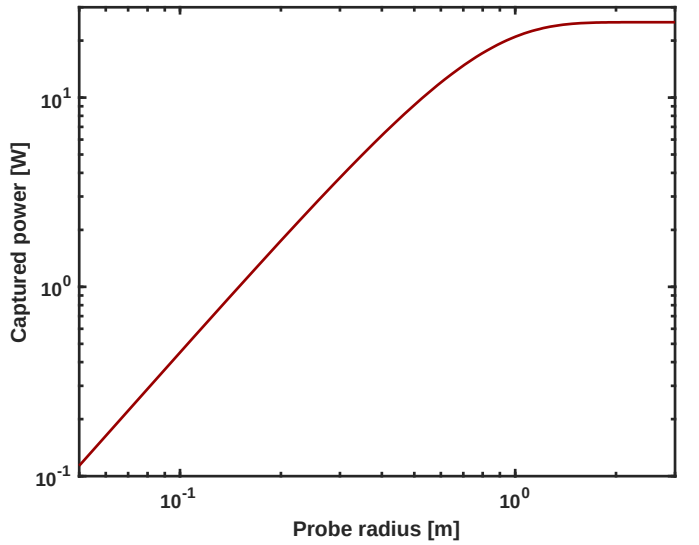

Figure 10: Integrated power from the laser beam impinging on a circular disc aligned with the beam center. Captured power at 1000 km over a range of probe sizes.

The limiting factor in size is the minimum amount of power required to operate the probe. The Stardust femtosatellite uses a CC2510 system on chip (SoC) with integrated processor and radio, running at 90 mW, and hosts a magnetometer payload that consumes 15 mW [44]. The Sprite chipsat, based around the CC430 SoC, uses a maximum of 77 mW with much of this power likely consumed by the radio transmitter [45]. SpaceChip, a preliminary design for a complete satellite

bus on a SoC, has a power budget of 1.14 mW, of which 1 mW is dedicated to communication [46]. These prior designs indicate that extremely low power operation of the probe is feasible.

This captured power is subject to a number of efficiency factors that reduce the available electrical power to the probe's systems. For a monochromatic laser, a single-junction photovoltaic cell can achieve relatively high efficiencies, compared to multi-junction cells designed for the solar spectrum. Typical conversion efficiencies of about 50% have been demonstrated for monochromatic light [47], with a recent demonstration of 68.9% efficiency [48] under 858 nm laser light. However, this record-breaking efficiency was achieved at an irradiance of 11.4 W/cm^2, or about 30,000 times the solar irradiance at Uranus. While lightweight membrane concentrators similar to those envisioned for space solar power satellites [49] can be used, the achievable concentration factor would likely be no more than 10 to 20 times. Assuming a photovoltaic conversion efficiency of 50%, and applying another 50% efficiency to account for offset pointing and reduced reflectivity for attitude control, this would allow the three probe sizes to operate at 5 W, 750 mW, and 25 mW, respectively, at 1000 km from the mothership. To achieve the 90 mW power level required by the Stardust femtosatellite, a capture area with a radius of approximately 9 cm would be required.

5.2 Translation authority and disturbance forces

The available power delivered from the laser beam to the probe is contingent on the probe remaining centered and aligned with the laser beam. An inclined orientation relative to the laser beam can provide, if the probe is sufficiently light, a transverse component of force to counter external disturbances and to actively remain centered in the beam. In general, photon pressure scales with total irradiance, divided by the speed of light *c*. The total force imparted on the probe by absorption of the laser light therefore follows a trend similar to the total captured power shown in Figure 9 above. For a perfectly reflective surface, the momentum transfer of the outgoing photons is aligned such that the total resultant force from incoming and outgoing light is directed in the surface normal direction. This force scales with the square of the cosine of the angle between the surface normal and the incoming laser beam. The squared cosine factor accounts both for the projection of area in the beam direction, and for the projection of the resultant force normal to the surface. For a non-ideal reflector, the specular reflection will be less than the incoming light, and there may be a diffuse reflection component to the resultant force [50]. As an upper bound, for a probe that is oriented normal to the laser beam and perfectly reflects the full 25 W output power, the imparted force from photon pressure is 0.167 μN.

In this study, we consider external forces from ambient solar radiation pressure and from non-Keplerian motion in orbit around Uranus. Solar radiation at a distance of 18.3 to 20.1 AU imparts a pressure of 11 to 13 nPa, varying with the Uranian season. The magnitude of this disturbance force depends, however, on the reflectivity of the probe as well as on the projected area relative to the sun direction. Non-Keplerian disturbance forces manifest in several ways, depending on the trajectory of the probe relative to the mothership. Figure 11 depicts the conditions for three of

these force components with the magnitude of separation greatly exaggerated to clarify the geometry.

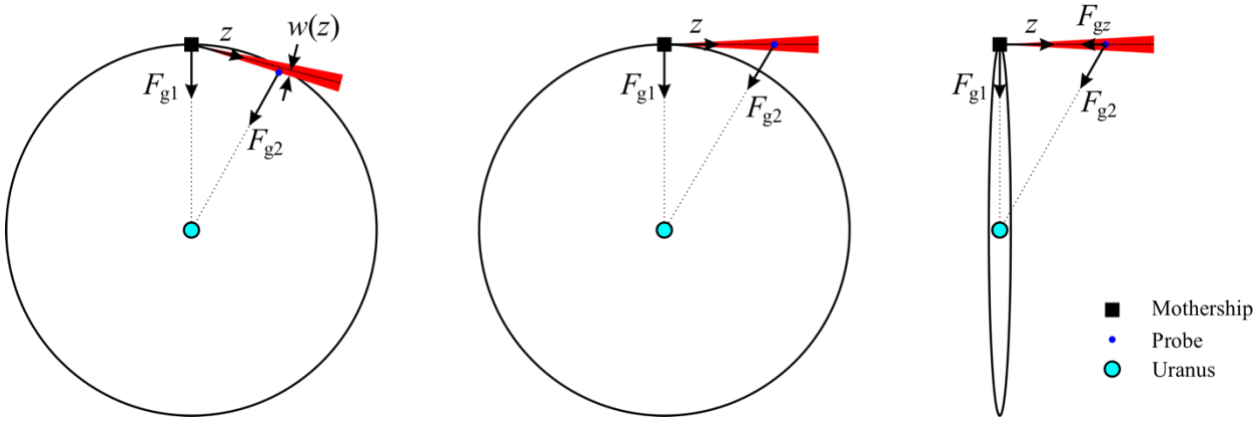

Figure 11: Geometry for three non-Keplerian orbital disturbance forces. Beamwidth gravity gradient force (left). z/R_{orb} gravity gradient force (center). Out-of-plane gravitational component (right). Here F_{g1} refers to the nominal gravitational force experienced by the probe when initially deployed, and F_{g2} refers to the gravitational force as the probe separates from the mothership.

First, if the probe is deployed in the along-track direction and maintains an orbital radius approximately equal to the mothership, then the extent to which it can navigate in the radial direction is constrained by the beam width, which increases with distance from the mothership (Figure 11, left). This "gravity gradient force" across the beam width (i.e., the difference in gravitational force felt by the mothership and the probe, which must be overcome by control of the reflected laser photon force) is

$$F_{gBW} = \left(\frac{GM}{(R_{orb} - w)^2} - \frac{GM}{R_{orb}^2} \right) m, \tag{10}$$

where GM is the gravitational parameter of Uranus, R_{orb} is the mothership's orbital radius around Uranus, and m is the mass of the probe.

However, if the laser beam is oriented perfectly in the along-track direction at the mothership, rather than tracking the probe as it travels ahead of or behind the mothership, then the probe would have to gradually increase its orbital radius to remain centered in the laser beam (Figure 11, center). This z/R_{orb} gravity gradient force is

$$F_{gZR} = \left(\frac{GM}{R_{orb}^2} - \frac{GM}{R_{orb}^2 + z^2} \right) m. \tag{11}$$

Finally, if the probe is deployed in a direction aligned with the orbit normal or anti-normal, and intended to maintain this transverse separation in an orbital plane that is parallel to the

mothership's but is offset from the planetary center of mass, then the laser must overcome the projection of the gravitational force in the orbit normal direction (Figure 11, right):

$$F_{\mathrm{gOOP}} = \frac{GM}{R_{\mathrm{orb}}^2}\frac{z}{R_{\mathrm{orb}}}m, \tag{12}$$

where z is assumed to be small compared to R_{orb}.

In Figure 12, these forces are plotted relative to the laser photon force as a function of separation from the mothership for an orbit at 23 R_{U} (583,318 km) and for the three reference probe sizes.

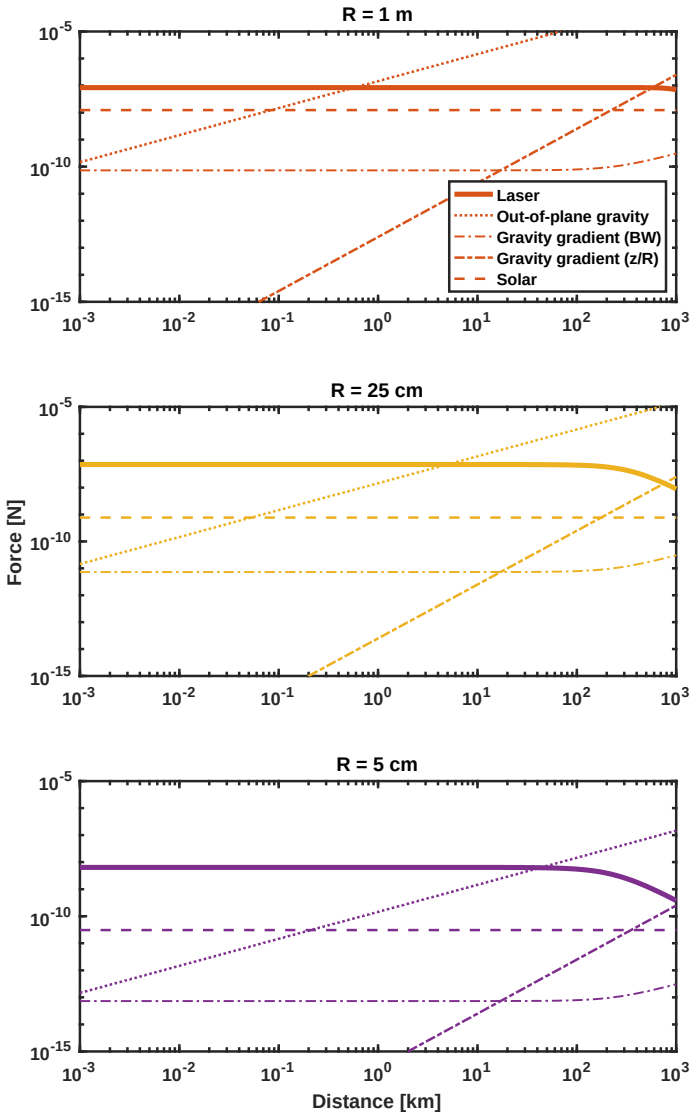

Figure 12: Laser photon force and disturbance forces plotted as a function of separation distance for three different probe sizes.

The laser photon force is plotted as $P(z)/c$, accounting for only one component of either photon absorption or reflection. Practically, the absorption force will always be aligned with the laser beam direction and only the reflection can be used to counter any transverse disturbances.

These trends make clear how challenging it is to deviate from a trajectory governed by Kepler's laws. While solar and the beam width gravity gradient force remain well below the laser photon force by at least an order of magnitude, the z/R_{orb} gravity gradient force exceeds the laser force for the larger probe sizes once it goes beyond several hundred kilometers from the mothership, and the out-of-plane gravitational component quickly exceeds the laser force at much smaller separation distances. In particular, even the lightest probe configuration can only sustain an orbital plane offset of approximately 40 km, which is well below the desired 1000 km operation range though potentially relevant for other distributed measurements beyond the scope of those considered in this study. It may be possible to implement an orbital plane change using the laser over multiple orbits, but this would require intermittent illumination that is inconsistent with using the laser for power transfer, and the challenge of pointing the laser and tracking the probe would become more difficult.

5.3 Attitude and thrust control

As described in the previous section, translational authority using laser photon pressure is dependent on attitude control of the probe to orient the reflector surface normal in a prescribed direction. This can also be achieved using laser photon pressure, but requires active management of the reflectivities on different probe surfaces in order to produce the desired torque. Electronic control of the surface reflectivity using thin-film liquid crystal devices (LCDs) on the order of 300 to 400 nm thickness [51] would add little mass to the probe, and can be driven with relatively low power consumption. Using reflectivity control based on thin film LCDs to implement attitude control has been demonstrated on the IKAROS solar sail [52] and was also envisioned as a means of attitude control for ultralight small spacecraft in orbit around near-Earth asteroids [53].

Compared to these prior attitude control concepts, a challenge that is unique to SCATTER is the need to maintain control in the presence of a non-uniform illumination. If the probe deviates too far from the laser beam center, there will be insufficient photon pressure to maintain active attitude control. To establish the envelope within which attitude control is possible, we calculate the torque exerted by the laser beam on square panels corresponding to the three probe sizes, as a function of distance from the laser beam center. For each probe size, we calculate this torque for three reflectivity conditions: the entire panel fully reflective, the left side reflective and the right fully absorbing, and the left side fully absorbing and right side reflective. These half-reflective "butterfly" configurations (each membrane half reminiscent of a butterfly wing) represent the limiting cases of torque that can be imposed by the laser. Figure 13 shows the torque profiles for each probe size, along with the response time as a function of probe position from the laser beam center.

The minimum required torque is specified based on the assumed response time for the corresponding probe size. For each probe size, the inertia was estimated by assuming a uniform

square chassis and a larger square membrane. The smallest probe was represented by a 1 gram, 10×10 cm membrane and a 4 gram, 4×4 cm planar chassis. The intermediate probe was represented by a 50 gram, 50×50 cm membrane and a 450 gram, 10×10×5 cm chassis. Finally, the largest probe was represented by a 500 gram, 2×2 m membrane and a 4500 gram, 10×10×30 cm chassis. The torque required to rotate this mass distribution over 45 degrees within an hour was determined to be the minimum acceptable torque for attitude control of the corresponding probe.

These torque profiles were calculated for a 50 cm width laser, i.e., close to the emitter before it starts to diverge. For the smallest probe size, deviations of up to 16.0 cm from the laser center will still yield torques in both directions that provide an acceptable rate of response. For the larger 50 cm probe, the controllable region shrinks to 4.11 cm from the laser beam center. The largest 2 m probe has a narrow region of 3.51 cm from the beam center where it is possible to achieve torques in both directions, but not with an acceptable response time.

Qualitatively, the difference in torque characteristics comes from the relative size of the probe compared to the laser beam. The smallest probe is several times smaller than the laser beam width, so across the span of the membrane there is less of a gradient in laser irradiance. As a result, the asymmetric reflectivity can achieve torques counter to the laser gradient when the probe is entirely on one size of the laser beam center. In contrast, the 2 m membrane is several times larger than the laser beam, and as it translates away from the beam center, the laser can effectively illuminate only one side of the probe, with no photon pressure on the other side to produce a counter-torque, regardless of reflectivity conditions. The much greater moment of inertia of the 5 kg chassis associated with the 2 m probe also drastically slows down the response for a given torque, compared to the 5 g chipsat.

As the probe's distance from the mothership increases, the increasing width of the laser beam will increase the size of the controllable region, since the fixed area reflectors will see a gentler gradient in irradiance. However, the overall magnitude of torque achievable will decrease as the peak irradiance drops, resulting in a slower response. Assuming that the probe is continuously under control, the initial deployment conditions should be the primary concern for transient response of the attitude control system; no sudden perturbative events would be expected as the probe traverses the 1000 km distance, so the gradually decreasing responsiveness is not a major concern.

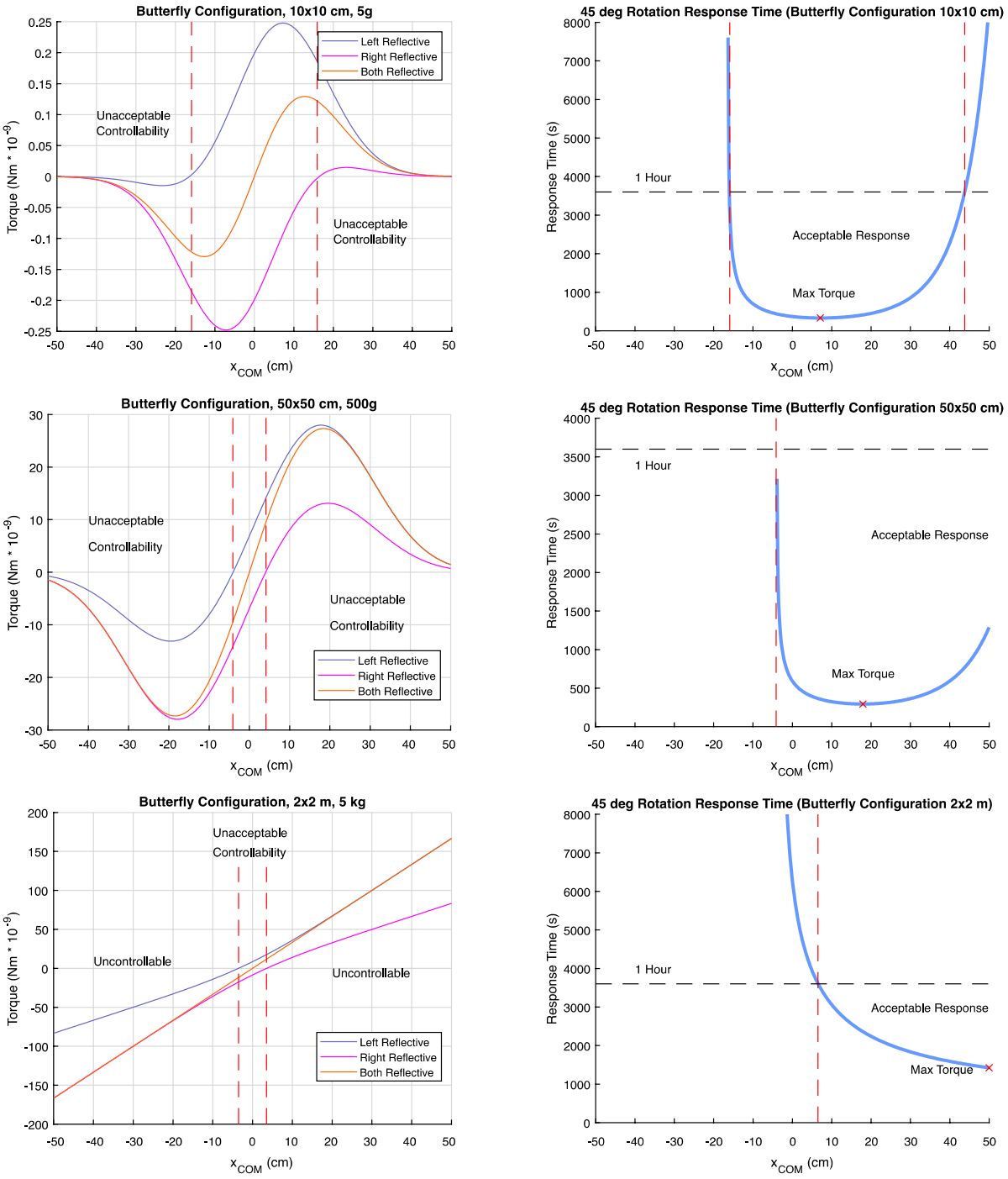

Figure 13: Asymmetric torque profiles (left) and response time (right) for probes of three sizes (top, middle, bottom).

5.4 Data transfer

In addition to transferring power from mothership to probe, the laser beam can also be used to transfer information between the two spacecraft. Laser communications has been demonstrated on numerous platforms in the Earth system for space-to-space, space-to-ground, and even space-to-aircraft communication links. In general, these lasers for communication are low power and can achieve high data rates. The first demonstration of space-based laser communication involved the aforementioned SILEX terminals on Artemis and SPOT-4 over a distance of 36,500 km [32]. This 60 mW laser demonstrated communication with a data rate of 50 Mbit/s. The European Data Relay System uses a Laser Communication Terminal that achieves data rates of 1.8 Gbit/s from Low Earth Orbit to Geosynchronous Earth Orbit (45,000 km) using a transmit power of 2.2 W. The Lunar Atmospheric Dust and Environment Explorer (LADEE) mission included the Lunar Laser Communication Demonstration (LLCD), which demonstrated duplex laser communication between lunar orbit and a ground station, over a distance of 385,000 km using a 0.5 W laser on the spacecraft [54]. At even greater distances, the MESSENGER (MErcury Surface, Space ENvironment, GEochemistry, and Ranging) spacecraft used the Mercury Laser Altimeter (MLA) to perform a laser ranging demonstration with a ground station over a distance of 24 million km [55].

Modulation of the 25 W outgoing laser from the mothership as a method of data transfer could be achieved either by switching the laser source or adjusting the optics. Assuming that the laser optics implement active thin film mirrors to take advantage of their low mass and shape correction capability [56], the optics can be rapidly defocused and refocused resulting in a variable irradiance impinging on the probe without rapid switching of the laser source itself. On the probe, a retroreflective panel on the probe would reflect light directly back to the mothership and could be detected to track the distance and position of the probe. An overlaid LCD similar to that used for attitude control in Section 5.3 would provide a mechanism for information transfer back to the mothership that is insensitive to probe orientation and could potentially be driven at microsecond timescales [57] corresponding to a raw data rate of hundreds of kilobits per second.

5.5 Probe lifetime and survivability

The lifetime of a deployed probe is primarily driven by the need to maintain operation to a distance of 1000 km from the mothership. The duration of this traversal is influenced by a number of factors including the laser photon pressure and orbital dynamics, but is most strongly determined by the initial separation speed imparted by the probe deployer.

Based on the passive spring deployment discussed in Section 4.2, a 5 kg probe in the form of a 3U CubeSat would deploy at an initial speed of approximately 1.5 m/s, corresponding to a kinetic energy of 5.6 J imparted by the deployment spring. For the smallest probe under consideration, the thousand-fold reduction in mass from 5 kg to 5 g would correspond to a deployment speed of 47 m/s using the same spring energy. This upper bound on the deployment speed, however, may be limited by a number of factors, including the shock tolerance of the smaller chipsat probes, the

structural tolerances of the deployer (especially if located coaxially on the laser secondary mirror mount), and the size of the spring that is compatible with a smaller probe area. For this initial analysis of the three reference probe sizes, we assume that the larger probes would use a deployment spring similar to existing CubeSat deployers, and therefore achieve deployment speeds that scale with the inverse square root of mass. The intermediate 500 g probe would therefore deploy with an initial speed of 4.7 m/s. For the chipsat sized probe, we limit the deployment speed to 10 m/s based on the considerations described above.

As the probe separates from the mothership, the force imparted by the laser beam will contribute additional thrust. This thrust, corresponding to the captured power divided by the speed of light, can be integrated over time to calculate the resulting change in probe speed. Figure 14 shows the speeds of the three probes over the 1000 km traversal, with very little contribution from photon pressure. The final speeds of the three probes are 1.51 m/s, 4.71 m/s, and 10.04 m/s, respectively. Neglecting orbital mechanics and considering only straight-line motion, these correspond to flight times of 7.69, 2.46, and 1.15 days to reach a distance of 1000 km, as shown in Figure 15.

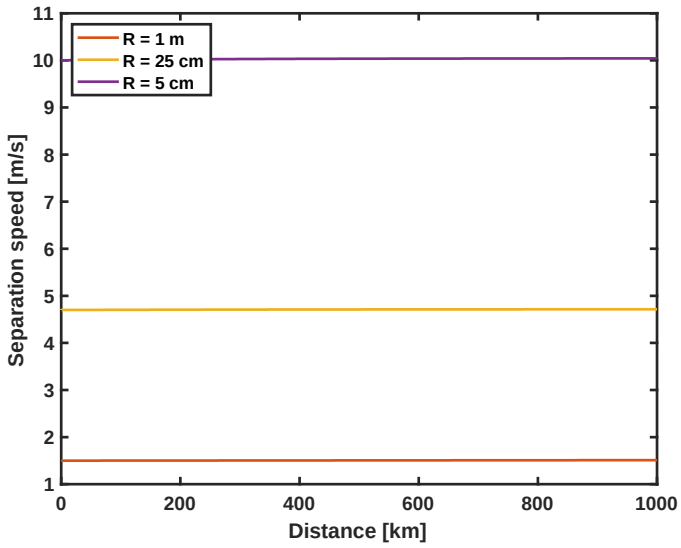

Figure 14: Separation speed as function of distance from the mothership for three probe sizes for nominal deployment speed.

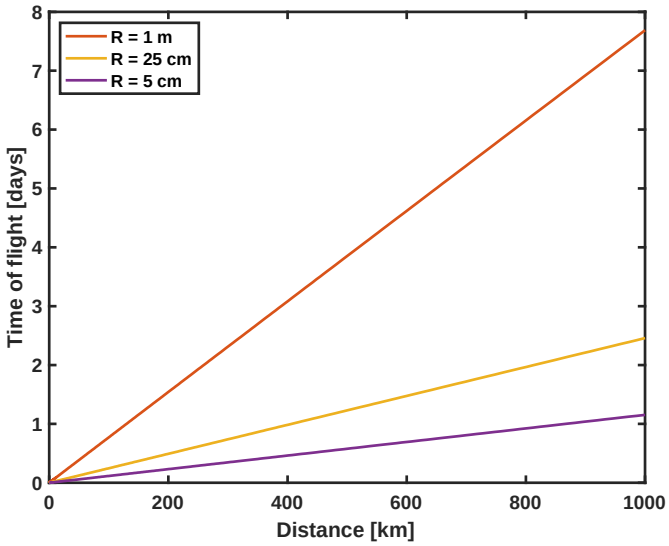

Figure 15: Time of flight as function of distance from the mothership for three probe sizes for nominal deployment speed.

If, instead of the 10 m/s deployment speed for the chipsat probe, we scale the CubeSat spring force to achieve an initial speed of 47 m/s, the chipsat would traverse the 1000 km distance in just under six hours. Compared to the 9.3 and 13.5 day periods of 18 R_U and 23 R_U orbits around Uranus, the flight time of the largest probe is long enough that the assumption of straight-line motion breaks down and the relative between probe and mothership is governed by the Hill–Clohessy–Wiltshire equations. As a rough approximation, changing the orbital speed by 1.5 m/s shifts the orbital radius on the opposite side by, coincidentally, about 1000 km. This would achieve the desired separation, but in a direction with a large radial component rather than along-track. Similarly to the out-of-plane motion described in Section 5.2, this relative motion may not be ideal for our goal of decoupling spatial and temporal variations in magnetospheric measurements, but may be useful for other distributed measurements.

In order to assess the maximum potential contribution of photon pressure to probe speed, we use the same analysis but with zero initial deployment velocity, which maximizes the duration of time spent in the region of greatest irradiance from the laser. For this bounding case, as shown in Figures 16 and 17, the laser imparts a velocity of 0.18 m/s, 0.37 m/s, and 0.92 m/s on the three probe sizes, corresponding to times of flight of 127 days, 48 days, and 17.6 days to reach 1000 km separation.

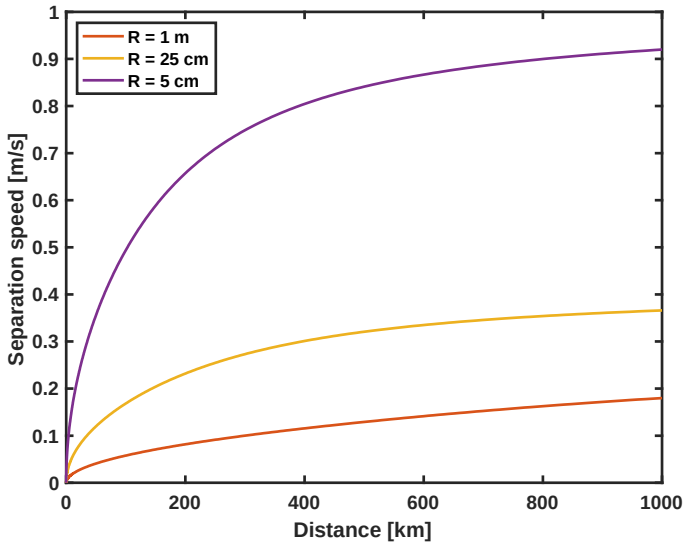

Figure 16: Separation speed as function of distance from the mothership for three probe sizes for zero initial deployment speed.

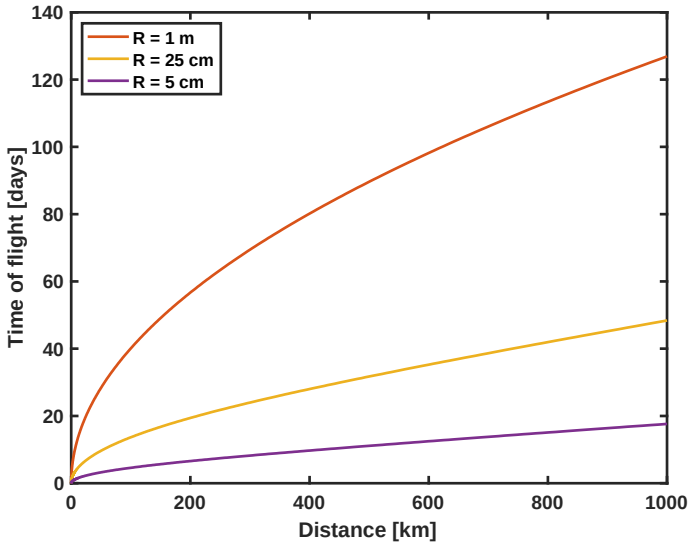

Figure 17: Time of flight as function of distance from the mothership for three probe sizes for zero initial deployment speed.

In both cases, we assume full reflectivity on the probe to provide an upper bound on the effect of the laser photon thrust; however, this would result in zero electrical power captured by the probe. The case of zero deployment velocity, while impractical, provides leeway for the design of the deployer system—we know that even with no spring force, a probe can eventually separate to 1000 km distance on photon pressure alone. This allows the deployment system to accommodate

potentially severe mass limitations, and to scale the deployment speed to satisfy other constraints, such as probe survivability in the radiation environment of Uranus.

The only in situ measurements of the Uranian radiation environment comes from the Voyager 2 flyby. Since the purpose of the SCATTER probes is to explore the environment surrounding the magnetopause and bow shock, the charged particle density will likely be highly variable over the lifetime of the probe. Voyager 2's low-energy charged-particle (LECP) instrument showed an increase in particle count by a factor of 100 in the vicinity of the bow shock, and ion intensities after crossing the magnetopause were about 1000 times greater than the interplanetary intensities [14]. JPL's recently developed Uranian Radiation Model [17] incorporates the Voyager LECP and TET (The Electron Telescope) measurements to provide a comprehensive picture of the radiation environment. This radiation model in general predicts a low concern for total ionizing dose (TID) beyond 8 R_U and a total dose of only 100 rads for a flyby following Voyager 2's trajectory using 100 mils (2.54 mm) of aluminum shielding. This is well below the TID threshold for many commercial off the shelf (COTS) components such as DC–DC converters that tolerate up to 15–20 krad TID and the ATSAMD51G microcontroller that showed onset of memory failure at 16 krad TID [58]. For the short flight time of any probe configuration, assuming that a deployment spring is used, minimal shielding will be required to address TID concerns. For the lightest probe configuration, the addition of shielding would also substantially increase the probe mass, and reduce its deployment speed. The trade-off between increased shielding and more rapid traversal is worth exploring in the future for a more detailed analysis of lifetime and survivability.

Once the probe travels beyond 1000 km from the mothership, we assume that it is no longer useful for making measurements and transmitting data in support of the scientific mission. However, the probe itself will remain in orbit around Uranus, and can potentially be a concern for planetary protection if it eventually lands on one of the moons in the vicinity. After the laser is no longer directed at the probe, solar radiation pressure is the dominant orbital perturbation that can affect the probe's orbit. As discussed above, solar radiation pressure at Uranus is approximately 12 nPa. Given the low areal density of the chipsat-sized probes, it is important to understand the long-term effect of these perturbations. For the 5 g probe with an area of 100 cm^2 in a circular orbit, the average acceleration due to solar radiation pressure over the period of the orbit can be as high as 4.93×10^{-8} m/s^2, assuming that the probe is fully reflective and remains facing the sun. This acceleration, aligned with the sun direction, introduces a bias to the orbit, since it increases the probe's speed over half the orbit and decreases the speed over the other half. Figure 18 show the effects of SRP on the eccentricity of two initially circular orbits at 18 and 23 R_U over 10 years.

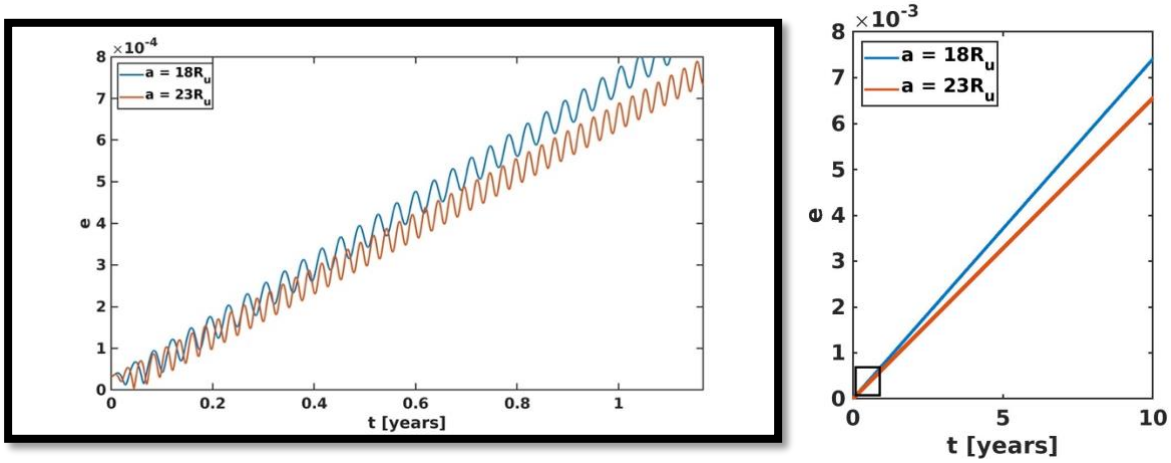

Figure 18: Increasing orbital eccentricity over 1 year (left) and 10 years (right) for two initially circular orbits at 18 and 23 R_U, under the influence of solar radiation pressure, for the chipsat-sized probe.

The increase in eccentricity from zero to about 0.007 shows that the SRP effects alone will not be great enough to significantly perturb a probe orbit such that it approaches one of the primary satellites. As a result, so long as the initial mothership orbit is sufficiently well isolated from any Uranian moon, the deployed probes will likewise avoid collisions with the same moons.

6 Conclusions

CubeSats alone will have difficulty exploring the outer solar system using conventional power sources like PV arrays and RTGs. SCATTER can enable exploration of the outer solar system, using small spacecraft to make distributed measurements, by providing a centralized power source and a communications relay for the probe spacecraft. This initial study assesses the feasibility of the SCATTER concept over a range of probe parameters including mass and size. From these results, we find that a medium-sized probe, corresponding roughly to a 0.5U CubeSat (10×10×5 cm) with a 0.5 m deployable membrane concentrator, achieves better performance than the two extreme cases in size. The larger probe has too large a deployable to make good use of the laser beam size and is too massive to maneuver using photon pressure. The smaller probe is extremely agile but would be more performance-limited because it does not capture a large enough fraction of the laser beam. The optimal probe size will ultimately be driven by the scientific payload's power requirements, imposing a minimum membrane concentrator area that factors in the need to divert some fraction of the impinging photon energy from electrical conversion to attitude control and communication. In this section, we review the major findings of the study and discuss avenues of future work to build on these results.

6.1 Summary of findings

A laser emitter on the mothership with a 26 cm aperture and 25 W output power is sufficient to exceed solar irradiance to a distance of 1000 km.

This aperture was selected to maintain an irradiance greater than the ambient solar irradiance of 3.69 W/m^2 in Uranian orbit out to a distance of 1000 km, assuming diffraction-limited divergence of a laser with a wavelength of 800 nm.

For probe sizes ranging from 5 grams to 5 kilograms, we find that an intermediate size corresponding to a 0.5U CubeSat achieves the best combination of performance metrics.

We assume that a 0.5U probe has a total mass of 500 grams, corresponding to a 50 gram, 50×50 cm membrane and a 450 gram, 10×10×5 cm chassis. This probe size, matched to the laser aperture, captures much of the transmitted laser power over the distance traversed, dropping from an initial 21 W to a minimum of 3 W at 1000 km distance. Even considering conversion efficiencies, this corresponds to nearly 1 W of steady-state power available. The intermediate probe size is also well-suited for maintaining attitude control using photon pressure. In comparison, the smaller probe is more agile and has greater tolerance on translation within the beam, but is constrained to operate on only 10s of mW at 1000 km distance because of its small capture area. The largest probe can capture most of the transmitted laser power out to the maximum distance, but is unable to navigate using photon pressure.

With a 50 x 50 cm deployable membrane, the intermediate probe size is capable of maintaining laser-based attitude control within about 4 cm of the beam centerline.

To establish the envelope within which attitude control is possible, we calculated the torque exerted by the laser beam on square panels corresponding to the three probe sizes, as a function of distance from the laser beam center and under three reflectivity conditions. This analysis established an envelope of achievable torques, in order to identify the region within which actuation authority in both directions is possible. Qualitatively, the difference in torque characteristics for the three probe sizes comes from their relative size compared to the laser beam.

Assuming spring-driven deployment, probes will traverse the 1000 km distance in 1 to 6 days, with little effect on time-of-flight from radiation pressure.

With deployment driven by a passive spring, similar to existing CubeSat deployers, the initial separation speeds range from 1.5 m/s to 47 m/s, depending on probe mass. The impinging laser photon pressure only adds about 0.5% to 1% of additional speed. This short flight time, regardless of probe configuration, means that minimal radiation shielding will be required to address total ionizing dose (TID) concerns. For the lightest probe configuration, the addition of shielding would also substantially increase the probe mass, and reduce its deployment speed.

6.2 Next steps

To further develop the viability of the SCATTER architecture, a more detailed design of the mothership and probe systems is required. The laser source, optics, and probe deployment mechanism require selection of particular technologies and configurations in order to provide a better estimate of the laser beam geometry over a distance of 1000 km. The geometry of the probe and its subsystems also require greater definition, including the arrangement of membrane concentrators, reflectivity control panels, and scientific payload.

The roadmap to elevating the technology readiness of SCATTER would first start with prototype fabrication for characterization of its performance in a laboratory environment. Subsequently, technology demonstration missions in Earth orbit or deployed from a lunar spacecraft or outpost could be used to raise the technology readiness level of the laser-driven probe concept. The development of WPT technologies such as SCATTER will also be applicable to enhancing the robustness of fractionated spacecraft concepts for Earth-orbiting swarms and constellations. Spacecraft using SCATTER would have the potential to support each other in the event of power failures. Laser-based remote manipulation of objects in space can also have applications in space debris management in low Earth orbit. These complementary concepts could serve as further validation of the SCATTER architecture prior to its implementation on a Uranus orbiter mission.

7 References

[1] Lee, N., Close, S., Goel, A., Lauben, D., Linscott, I., Johnson, T., Strauss, D., Bugiel, S., Mocker, A., and Srama, R., "Theory and experiments characterizing hypervelocity impact plasmas on biased spacecraft materials," *Physics of Plasmas*, Vol. 20, 032901, 2013. doi: 10.1063/1.4794331

[2] Close, S., Linscott, I., Lee, N., Johnson, T., Strauss, D., Goel, A., Lauben, D., Srama, R., Mocker, A., and Bugiel, S., "Detection of electromagnetic pulses produced by hypervelocity micro particle impact plasmas," *Physics of Plasmas*, Vol. 20, No. 092102, 2013, pp. 1–8. doi:10.1063/1.4819777

[3] Young, S. A. Q., Lee, N., and Close, S., "Harvesting Electromagnetic Energy from Hypervelocity Impacts for Solar System Exploration," *URSI GASS*, Rome, Italy, 2020. doi: 10.23919/URSIGASS49373.2020.9232364

[4] Young, S. A. Q., Close, S., and Lee, N., "The Space Environmental Electrical Power Subsystem (SEEPS): Energy harvesting supporting microsatellite exploration of the outer solar system," *International Astronautical Congress*, Article IAC-19_C3_4_10_x54563, Washington, DC, 21–25 Oct., 2019.

[5] Young, S. A. Q., Stupl, J., Lee, N., and Close, S., "Theory of Power Generation from Spacecraft Charging," *IEEE Transactions on Plasma Science*, in press, 2021. doi: 10.1109/TPS.2021.3125709

[6] National Research Council, "The Giant Planets: Local Laboratories and Ground Truth for Planets Beyond," *Vision and Voyages for Planetary Science in the Decade 2013-2022*, The National Academies Press, 2013, pp. 175–216. doi: 10.17226/13117

[7] Arridge, C. S. et al., "The science case for an orbital mission to Uranus: Exploring the origins and evolution of ice giant planets," *Planetary and Space Science*, Vol. 104, 2014, pp. 122–140. doi: 10.1016/j.pss.2014.08.009

[8] Poleski, R., Gaudi, B. S., Udalski, A., Szymański, M. K., Soszyński, I., Pietrukowicz, P., Kozłowski, S., Skowron, J., Wyrzykowski, Ł., and Ulaczyk, K., "An ice giant exoplanet interpretation of the anomaly in microlensing event OGLE-2011-BLG-0173," *The Astronomical Journal*, Vol. 156, No. 104, 2018, pp. 1–11. doi: 10.3847/1538-3881/aad45e

[9] Ness, N. F., Acuna, M. H., Behannon, K. W., Burlaga, L. F., Connerney, J. E. P., Lepping, R. P., and Neubauer, F. M., "Magnetic Fields at Uranus," *Science*, Vol. 233, No. 4759, 1986, pp. 85–89. url: https://www.jstor.org/stable/1697500

[10] Masters, A., "Magnetic reconnection at Uranus' magnetopause," *Journal of Geophysical Research: Space Physics*, Vol. 119 No. 7, 2014, pp. 5520–5538. doi: 10.1002/2014JA020077

[11] Behannon, K. W., Acuna, M. H, Burlaga, L. F., Lepping, R. P., Ness, N. F., and Neubauer, F. M., "Magnetic Field Experiment for Voyagers 1 and 2," *Space Science Reviews*, Vol. 21, 1977, pp. 235–257. doi: 10.1007/BF00211541

[12] Krimigis, S. M., Armstrong, T. P., Axford, W. I., Bostrom, C. O., Fan, C. Y., Gloeckler, G., and Lanzerotti, L. J., "The low energy charged particle (LECP) experiment on the Voyager spacecraft," *Space Science Reviews*, Vol. 21, No. 3, 1977, pp. 329–354. doi: 10.1007/BF00211545

[13] Stone, E. C., Vogt, R. E., McDonald, F. B., Teegarden, B. J., Trainor, J. H., Jokipii, J. R., and Webber, W. R., "Cosmic ray investigation for the Voyager missions; energetic particle studies in the outer heliosphere—And beyond," *Space Science Reviews*, Vol. 21, No. 3, 1977, pp. 355–376. doi: 10.1007/BF00211546

[14] Krimigis, S. M., Armstrong, T. P., Axford, W. I., Cheng, A. F., Gloeckler, G., Hamilton, D. C., Keath, E. P., Lanzerotti, L. J., and Mauk, B. H. "The magnetosphere of Uranus: Hot plasma and radiation environment", *Science*, Vol. 233, No. 4759, 1986, pp. 97–102. doi: 10.1126/science.233.4759.97

[15] Lanzerotti, L. J., Brown, W. L., Maclennan, C. G., Cheng, A. F., Krimigis, S. M., and Johnson, R. E., "Effects of charged particles on the surfaces of the satellites of Uranus," *Journal of Geophysical Research: Space Physics*, Vol. 92, No. A13, 1987, pp. 14949–14957.
doi: 10.1029/JA092iA13p14949

[16] DiBraccio, G. A. and Gershman, D. J., "Voyager 2 constraints on plasmoid-based transport at Uranus," *Geophysical Research Letters*, Vol. 46, No. 19, 2019, pp. 10710–10718.
doi: 10.1029/2019GL083909

[17] Garrett, H., Martinez-Sierra, L. M., and Evans, R, "The JPL Uranian Radiation Model (UMOD)", JPL Publication 15-7, Pasadena, CA, 2015.
url: http://hdl.handle.net/2014/45462

[18] Cao, X. and Paty, C., Asymmetric Structure of Uranus' Magnetopause Controlled by IMF and Planetary Rotation. Geophysical Research Letters, Vol. 48, No. 4, 2021, e2020GL091273.
doi: 10.1029/2020GL091273

[19] Walsh, A. P., Fazakerley, A. N., Lahiff, A. D., Volwerk, M., Grocott, A., Dunlop, M. W., Lui, A. T. Y., Kistler, L. M., Lester, M., Mouikis, C., Pu, Z., Shen, C., Shi, J., Taylor, M. G. G. T., Lucek, E., Zhang, T. L., and Dandouras, I., "Cluster and Double Star multipoint observations of a plasma bubble," *Annales Geophysicae*, Vol. 27, 2009, pp. 725–743.
doi: 10.5194/angeo-27-725-2009

[20] Donovan, E. et al., "The THEMIS all-sky imaging array — system design and initial results from the prototype imager," *Journal of Atmospheric and Solar-Terrestrial Physics*, vol. 68, 2006, pp. 1472–1487.
doi: 10.1016/j.jastp.2005.03.027

[21] Jarmak, S., et al., "QUEST: A New Frontiers Uranus orbiter mission concept study," *Acta Astronautica*, Vol. 170, 2020, pp. 6–26.
doi: 10.1016/j.actaastro.2020.01.030.

[22] Balint, T. et al., "Uranus System Exploration Under the New Frontiers Mission Class (A Novel Perspective)," *Bulletin of the American Astronomical Society*, Vol. 53, No. 4, 2021, 040.
doi: 10.3847/25c2cfeb.5f581eff

[23] Hofstdater, M. et al., "Ice Giants Pre-Decadal Survey Mission Study Final Report," JPL Publication D-100520, Pasadena, CA, 2017.
url: https://www.lpi.usra.edu/icegiants/mission_study/Full-Report.pdf

[24] Bridge, H. S. et al., "Plasma observations near Uranus: Initial results from Voyager 2," *Science*, Vol. 233 No. 4759, 1986, pp. 89–93.
doi: 10.1126/science.233.4759.89

[25] Ritz, F. and Peterson, C. E., "Multi-mission radioisotope thermoelectric generator (MMRTG) program overview," *IEEE Aerospace Conference Proceedings*, Vol. 5, 2004,

pp. 2950–2957.
doi: 10.1109/AERO.2004.1368101

[26] Vandermey, N. and Paczkowski, B. G., "The Cassini-Huygens Mission Overview," *AIAA SpaceOps Conference*, No. AIAA 2006-5502, 2006.
doi: 10.2514/6.2006-5502

[27] Summerer, L. and Purcell, O., "Concepts for wireless energy transmission via laser," European Space Agency (ESA)-Advanced Concepts Team, 2009.

[28] Shreck, S. and Latifi, S., "Wireless Power Transmission," *Proceedings of the International Conference on Information and Knowledge Engineering (IKE)*, 2011.

[29] Alda, J., "Laser and Gaussian Beam Propagation and Transformation," *Encyclopedia of Optical Engineering*, 2003.
doi: 10.1081/E-EOE 120009751

[30] Landis, G. A., "Laser power beaming for lunar polar exploration," *AIAA Propulsion and Energy Forum*, 2020, pp. 1–6.
doi: 10.2514/6.2020-3538

[31] Bennett, G. L., "Space Nuclear Power: Opening the Final Frontier," *4th International Energy Conversion Engineering Conference and Exhibit (IECEC)*, No. AIAA 2006-4191, San Diego, CA, 2006.
doi: 10.2514/6.2006-4191

[32] Tolker-Nielsen, T. and Oppenhauser, G., "In-orbit test result of an operational optical intersatellite link between ARTEMIS and SPOT4, SILEX," *Proc. SPIE, Free-Space Laser Communication Technologies XIV*, Vol. 4635, 2002.
doi: 10.1117/12.464105

[33] Nakagawa, K. and Yamamoto, A., "Preliminary design of Laser Utilizing Communications Equipment (LUCE) installed on Optical Inter-Orbit Communications Engineering Test Satellite (OICETS)," *Proc. SPIE, Free-Space Laser Communication Technologies VII*, Vol. 2381, 1995.
doi: 10.1117/12.207415

[34] Jono, T. et al., "In-orbit test results of the inter satellite laser link by OICETS," *AIAA International Communications Satellite Systems Conference*, 2007.
doi: 10.2514/6.2007-3116

[35] Steeves, J., Laslandes, M., Pellegrino, S., Redding, D., Bradford, S. C., Wallace, J. K., and Barbee, T., "Design, fabrication and testing of active carbon shell mirrors for space telescope applications," *Proc. SPIE, Advances in Optical and Mechanical Technologies for Telescopes and Instrumentation*, Vol. 9151, No. 915105, 2014.
doi: 10.1117/12.2056560

[36] Wei, Y. and Pellegrino, S., "Modular Foldable Surfaces: a Novel Approach Based on Spatial Mechanisms and Thin Shells," *4th AIAA Spacecraft Structures Conference*, Grapevine, TX, 2017.
doi: 10.2514/6.2017-1345

[37] Puig-Suari, J., Schoos, J., Turner, C., Wagner, T., Connolly, R., and Block, R. P., "CubeSat developments at Cal Poly: the standard deployer and PolySat," *Proc. SPIE, Small Payloads in Space*, Vol. 4136, 2000.
doi: 10.1117/12.406645

[38] Blanchard, J. T., Anderson, B. D., Lo, M. W., and Close, S., "Low energy capture into high inclination orbits for ocean worlds missions," *AAS/AIAA Astrodynamics Specialist Conference*, 2020.

[39] Blanchard, J. T., Lo, M. W., Landau, D., and Anderson, B. D., "Invariant Funnels for Resonant Landing Orbits," *AAS Space Flight Mechanics Meeting*, 2021, pp. 1–17.

[40] Lee, N. and Pellegrino, S., "Multi-layered membrane structures with curved creases for smooth packaging and deployment," *AIAA Space Structures Conference*, National Harbor, Maryland, 2014.
doi: 10.2514/6.2014-1037.

[41] Lee, N. and Close, S., "Curved pleat folding for smooth wrapping," *Proceedings of the Royal Society A*, Vol. 469, 2013, 20130152.
doi: 10.1098/rspa.2013.0152.

[42] Arya, M., Lee, N., and Pellegrino, S., "Wrapping thick membranes with slipping folds," *AIAA Space Structures Conference*, Kissimmee, FL, 2015.
doi: 10.2514/6.2015-0682.

[43] "Power Via Laser," *SPIE Professional*, Vol. 9, No. 1, Jan 2014.

[44] Yang, L., Guo, J., Fan, C., Song, X., Wu, S., and Zhao, Y., "The design and experiment of stardust femto-satellite," *Acta Astronautica*, Vol. 174, 2020, pp. 72–81.
doi: 10.1016/j.actaastro.2020.04.034

[45] Manchester, Z., Peck, M., and Filo, A., "KickSat: A crowd-funded mission to demonstrate the world's smallest spacecraft," *AIAA/USU Conference on Small Satellites*, Paper SSC13-IX-5, 2013.

[46] Barnhart, D. J., Vladimirova, T., and Sweeting, M. N., "Very-Small-Satellite Design for Distributed Space Missions," *Journal of Spacecraft and Rockets*, Vol. 44, No. 6, 2007, pp. 1294–1306.
doi: 10.2514/1.28678

[47] Green, M. A., "Limiting Photovoltaic Monochromatic Light Conversion Efficiency," *Progress in Photovoltaics: Research and Applications*, Vol. 9, 2001, pp. 257–261.
doi: 10.1002/pip.375

[48] Helmers, H., Lopez, E., Höhn, O., Lackner, D., Schön, J., Schauerte, M., Schachtner, M., Dimroth, F., and Bett, A. W., "68.9% Efficient GaAs-Based Photonic Power Conversion Enabled by Photon Recycling and Optical Resonance," *Physica Status Solidi Rapid Research Letters*, Vol. 15, 2021, 2100113.
doi: 10.1002/pssr.202100113

[49] Arya, M., Lee, N., and Pellegrino, S., "Ultralight Structures for Space Solar Power Satellites," *3rd AIAA Spacecraft Structures Conference*, No. AIAA 2016-1950, San Diego,

California, USA, 2016.
doi: 10.2514/6.2016-1950.

[50] Campbell, B., A. and Thomas, S. J., "Realistic Solar Sail Thrust," *Advances in Solar Sailing*, edited by M. Macdonald, Springer Praxis Books, Berlin, 2014, pp. 407–435.
doi: 10.1007/978-3-642-34907-2_27

[51] Bobrov, Y., Fennell, L., Lazarev, P., Paukshto, M., and Remizov, S., "The manufacture of a thin-film LCD," *Journal of the Society for Information Display*, Vol. 10, No. 4, 2002, 317.
doi: 10.1889/1.1827884

[52] Saiki, T., Tsuda, Y., Funase, R., Mimasu, Y., Shirasawa, Y., and IKAROS Demonstration Team, "Attitude operation results of solar sail demonstrator IKAROS," *28th International Symposium on Space Technology and Science*, 2012.
doi: 10.2322/tastj.10.To_4_1.

[53] Lee, N. and Close, S., "Meteoroid Impact Detection for Exploration of Asteroids: Small satellites for asteroid characterization," *Journal of Spacecraft and Rockets*, Vol. 55, No. 1, 2018, pp. 202–213.
doi: 10.2514/1.A33928

[54] Boroson, D. M., Robinson, B. S., Murphy, D. v., Burianek, D. A., Khatri, F., Kovalik, J. M., Sodnik, Z., and Cornwell, D. M., "Overview and results of the Lunar Laser Communication Demonstration," *Free-Space Laser Communication and Atmospheric Propagation XXVI*, Vol. 8971, 2014, 89710S.
doi: 10.1117/12.2045508

[55] Smith, D. E., Zuber, M. T., Sun, X., Neumann, G. A., Cavanaugh, J. F., McGarry, J. F, and Zagwodzki, T. W., "Two-Way Laser Link over Interplanetary Distance," *Science*, Vol. 311, No. 5757, 2006, p. 53.
doi: 10.1126/science.1120091

[56] Laslandes, M., Pellegrino, S., Steeves, J., and Patterson, K., "Optimization of electrode configuration in surface-parallel actuated deformable mirrors," *Proc. SPIE, Adaptive Optics Systems IV*, Vol. 9148, No. 914843, 2014.
doi: 10.1117/12.2056495

[57] Lu, C.-W., Yin, P.-Y., Hsiao, C.-M., and Chang, M.-C. F., "A 10b Resistor-Resistor-String DAC with Current Compensation for Compact LCD Driver ICs", *IEEE International Solid-State Circuits Conference*, San Francisco, CA, 2011, pp. 318–320.
doi: 10.1109/ISSCC.2011.5746336

[58] Holliday, M., Ramirez, A., Settle, C., Tatum, T., Senesky, D., and Manchester, Z., "PyCubed: An Open-Source, Radiation-Tested CubeSat Platform Programmable Entirely in Python," *AIAA/USU Conference on Small Satellites*, Paper SSC19-WKIII-04, 2019.